DE GRUYTER OPEN

Acta Geophysica
vol. 63, no. 6, Dec. 2015, pp. 1516-1539
DOI: 10.1515/acgeo-2015-0061

An Analysis of Turbulent Heat Fluxes and the Energy Balance During the REFLEX Campaign

Christiaan van der TOL[1], Wim TIMMERMANS[1], Chiara CORBARI[2], Arnaud CARRARA[3], Joris TIMMERMANS[1], and Zhongbo SU[1]

[1]Department of Water Resources, Faculty ITC, University of Twente, Enschede, The Netherlands; e-mail: c.vandertol@utwente.nl

[2]Department of Hydraulic, Environmental and Surveying Engineering, Politecnico di Milano, Milano, Italy

[3]CEAM, Fundación de la Comunidad Valenciana
Centro de Estudios Ambientales del Mediterraneo, Paterna, Spain

Abstract

Three eddy covariance stations were installed at the Barrax experimental farm during the Land-Atmosphere Exchanges (REFLEX) airborne training and measurement campaign to provide ground truth data of energy balance fluxes and vertical temperature and wind profiles. The energy balance closure ratio (EBR) was 105% for a homogeneous camelina site, 86% at a sparse reforestation site, and 73% for a vineyard. We hypothesize that the lower closure in the last site was related to the limited fetch. Incorporating a vertical gradient of soil thermal properties decreased the RMSE of the energy balance at the camelina site by 16 W m^{-2}. At the camelina site, eddy covariance estimates of sensible and latent heat fluxes could be reproduced well using mean vertical profiles of wind and temperature, provided that the Monin–Obukhov length is known. Measured surface temperature and sensible heat fluxes suggested high excess resistance for heat (kB^{-1} = 17).

Key words: eddy covariance, SEB modelling, soil heat flux, surface roughness.

1. INTRODUCTION

Quantifying surface energy fluxes is relevant for boundary layer meteorology, climatology, ecology, hydrology, and agronomy. In those fields, the spatial variability of evapotranspiration and sensible heat is of great importance. Remote sensing techniques may assist in obtaining spatial estimates of these fluxes through radiometric observations. However, as fluxes cannot be observed directly, the remote sensing observations always have to be combined with models. One class of these models (among others, see Cleugh *et al.* 2007) are surface energy balance (SEB) models. SEB models that calculate land-atmosphere exchanges of energy and matter rely on observations of the temperature gradient between the land surface and the air to estimate the turbulent exchange of sensible and latent heat from surface to atmosphere (for a review, see Kalma *et al.* 2008).

These SEB models, however, are relatively "simple" models, and consequently their applicability needs to be carefully assessed. In particular, two parameters are of key importance: the difference between the surface and air temperature, and the aerodynamic resistance.

One of the problems of SEB models is that the difference between surface and air temperature can be relatively small, and thus prone to errors (Cleugh *et al.* 2007). Air temperature data are not available at the same spatial resolution as surface temperature, and often not even at the same time (Kustas and Norman 1996). Horizontal interactions within and between pixels are usually ignored, while this is not always justified (Gash 1987). Dual source models, used for pixels with partial vegetation cover (*e.g.*, Kustas *et al.* 1996), only partly solve this problem as, even in these schemes, horizontal fluxes are poorly represented and between-pixel interactions ignored. Timmermans *et al.* (2008) studied the effect of feedback mechanisms between fluxes on the one hand, and the surface to air temperature gradient on the other hand, by means of large eddy simulation (LES). They found a negative feedback between fluxes and the temperature gradient, which causes the extreme fluxes (lowest and highest values) to dampen. Models that do not include such interaction and that, for example, use a constant value or interpolated map for air temperature as input, may thus overestimate the extremes of sensible heat flux, which directly propagates into the estimate of latent heat flux and leads to errors in the estimates of vegetation water use.

Another problem with remote sensing driven land surface models is that the aerodynamic resistance for heat is difficult to estimate. The resistance for matter can be calculated from a wind profile, but estimating the resistance for heat requires extrapolation of the logarithmic vertical air temperature profile to the radiometrically measured temperature. The virtual height at which the extrapolated temperature equals surface temperature, z_{0h}, is usually

smaller than the roughness height for momentum, z_{0m} (Su *et al.* 2001). The ratio z_{0h}/z_{0m} can be expressed as an excess resistance (Owen and Thomson 1963), but several studies have shown that this excess resistance varies widely (Stewart *et al.* 1994, Verhoef *et al.* 1997, Massman 1999), in particular in areas with partial vegetation cover (Gökmen *et al.* 2012).

Both problems can be addressed if accurate measurements of temperature gradients and fluxes are available. The data collected during the Land-Atmosphere Exchanges (REFLEX) airborne training and measurement campaign at the Las Tiesas experimental farm in Spain serve this purpose. The area where the campaign took place is heterogeneous, due to the presence of irrigated agriculture in an otherwise naturally dry environment (Su *et al.* 2008). Although REFLEX was not the first airborne campaign at the farm, it had the unique aspect that the flights were optimized to provide information needed to study the heterogeneity of land-atmosphere fluxes of energy and water (Timmermans *et al.* 2014). The combination of high resolution airborne and ground data makes it possible to evaluate land surface models and model concepts at fine spatial resolution.

The objectives of the present paper are: (i) to evaluate the quality of eddy covariance collected during the REFLEX campaign, and (ii) to provide local estimates of surface fluxes, resistances, and vertical profile weather data. The paper describes results from three eddy covariance (EC) flux towers established for ground truth data collection at the experimental site between 17 and 29 July 2012. The focus of the present study is on one of the sites, where instrumentation was most elaborate. Of particular importance for later use in LES simulations were accurate local estimates of the surface energy balance fluxes, and vertical profiles of wind speed, temperature, and humidity in the vegetation and surface layer. Because the instruments were placed close to the surface, we were able to measure the energy balance of individual fields with a fairly homogeneous fetch at the stations, except for a station in a vineyard. We analyse the energy balance at the stations, address potential problems of energy balance closure, and verify the quality of measurements of vertical gradients of wind u, relative humidity RH, and air temperature T_a (Section 3.4), and radiometric surface temperature (Section 3.5) by estimating sensible and latent heat flux from profile data.

2. SITE DESCRIPTION AND INSTRUMENTATION

The study site is located in the La Mancha region in Spain, 20 km west of the city of Albacete. The experimental farm of Las Tiesas (also known as Barrax site) is located in a dryland area of which about 35% is used for irrigated agriculture, the remainder is either bare land or used for extensive, rain fed agriculture. The experimental farm is located on a (flat) plateau of about 700 m above mean sea level. The ground water level is about 20-30 m below

(a) (b) (c)

Fig. 1. Photographs of the three stations: (a) camelina field, (b) reforestation, and (c) vineyard.

Table 1

Instrumentation used at the three flux tower sites

Site name coordinates (WGS84)	Camelina 39.04109°N 2.08246°W	Reforestation 39.05975°N 2.08708°W	Vineyard 39.0598°N 02.2.1009°W
Dataloggers	CR5000, CR800 (Campbell Sci. Inc., USA) HOBO temperature dataloggers (Onset, USA) Degacon datalogger	CR23X, CR3000 (Campbell Sci. Inc., USA)	Fit-PC (EC), CR3000 with AM16/32 and AM25T multiplexers (Campbell Sci. Inc., USA)
Radiometers	CNR1 four component (Kipp and Zonen, Delft, Netherlands)	IRTS Apogee infrared temperature sensor	ThermoHygrometer (Thies Clima) at 2.50, 3.50, and 5.00 m height
Air temperature and relative humidity	CS215 (Campbell Sci. Inc., USA) at 1.20, 2.20, and 4.10 m height	CS215 (Campbell Sci. Inc., USA) at 1.45, 2.50, and 4.00 m height	2D Wind Sonic (Gill) at 2.50, 3.50, and 5.00 m height
Wind speed	Gill 2D at 5.20 m height	Cup anemometers Gill at 1.45, 2.50, and 4.00 m height	R3-50 (Gill) at 5.7 m height
Sonic anemometers	CSAT3 (Campbell Sci. Inc., USA) at 2.38 and 1.30 m height. Azimuth: 165° from N	Young 81000 at 5.00 m height (top of mast)	Sonic anemometer Young 81000 (top of mast)
Gas analysers	LI7500 at 2.38 m height	LI7500 at 5.00 m height	LI7500 at 5.70 m height
Soil tempera-ture	Onset soil temperature sensors at 1, 2, 4, 8, 16, and 32 cm depth		3x PT100 between 0 and 5 cm depth
Soil heat flux	Hukseflux (HFP01) at 8 and 13 cm depth	Hukseflux (HFP01) at 10 cm depth	Hukseflux (HFP01) at 2 cm depth
Soil moisture content	Degacon soil moisture sensors	CS616 at 10 cm depth	

the surface (Su *et al.* 2008). The three eddy covariance sites (Fig. 1) were located less than 2 km apart (see Timmermans *et al.* 2014), but in rather different land cover types (Table 1): a senescent camelina (*Camelina sativa*) field (0.5 m height), a reforestation plantation (bare soil and sparse trees of 1 to 3 m height), and a drip irrigated vineyard (about 1.8 m heigh).

2.1 Climate

The climate is Mediterranean (Köppen classification: Csa); the monthly average temperatures range from 11 °C (January) to 25 °C (July), and the mean annual rainfall is 400 mm. April, May, October, and November are the wettest months (~40-50 mm rainfall per month), and July and August the driest (~15 mm rainfall per month). The wind direction during the field campaign was predominantly southeast (Fig. 2). Mid-day air temperatures ranged from 31 to 38 °C, and night temperatures from 14 and 19 °C. The wind speed at 2.38 m height varied from 0.2 to 6.7 m s^{-1}, and the mean and standard deviations of wind speed were 3.0 and 1.6 m s^{-1}, respectively. The relative humidity ranged from 6% (midday) to 96% (night).

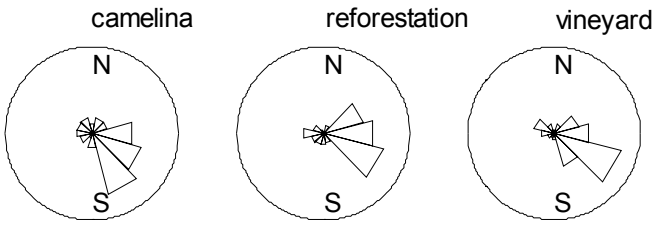

Fig. 2. Rose diagrams of wind direction at the three eddy covariance sites during the REFLEX campaign.

2.2 Instrumentation

At the three flux tower sites, the turbulent heat exchange, net radiation, and ground heat flux were estimated from measurements with the equipment listed in Table 1. Comparable equipment was used at each site. At each station, an eddy covariance system with 3-D sonic anemometer and gas analyser was installed. The dataloggers at the flux stations were programmed to collect the eddy covariance data at 20 Hz. The raw data were stored at the vineyard and camelina sites, while processed data were stored at the reforestation site. All other measurements were carried out at 0.2 Hz, and 1-minute averages were stored.

Wind speed, temperature, and relative humidity were measured at three or four heights above the surface at the flux tower sites. The sonic anemometers were installed at the top of the tower in the reforestation and vineyard

site, and at the south side of the tower at the camelina site (due to a different tower construction and mounting system). The gas analyser was located 20 cm northwest of the sonic anemometer at the camelina site, about 15 cm south at the reforestation site, and about 15 cm north at the vineyard site (see Fig. 1). The instrumentation at the camelina site was most complete. For this reason, the camelina site has been used for detailed analysis of the individual energy balance components.

3. METHODOLOGY

3.1 Turbulent heat fluxes and surface roughness

The turbulent heat fluxes (H and λE) were calculated with the software AltEddy (Alterra, WUR, Netherlands), ver. 3.71 (http://www.climatexchange.nl/projects/alteddy/) for the camelina and vineyard sites. The wind vector was double rotated for each averaging interval separately: horizontally rotated into the main wind direction (first rotation) and vertically (second rotation) so that average lateral and vertical wind speeds were zero. Furthermore, the following corrections were performed: de-spiking, 2-D axis rotation, WPL (Webb *et al.* 1980) correction, SND (Schotanus *et al.* 1983) correction, and a frequency response correction. The exact formulation for the frequency response correction as applied in AltEddy was not known, but for comparison Eqs. 11-13 in Horst (1997) were applied manually using the sampling frequency of 20 Hz, measurement height, wind speed, and Monin–Obukhov length as input. Due to the high measurement frequency and the low wind speed, the frequency response losses were small (around 2%). Tests for steady state within each averaging interval and integral turbulence characteristics have been carried out (Foken *et al.* 2005), and an overall quality flag was assigned according to Table 9.5 therein. Fluxes with an overall quality flag higher than 3 were rejected. In this way it was ensured that only data of high quality were included in the analysis, but this was still the majority of the half-hourly measurements in the time series.

At the reforestation site, flux calculations were carried out on the datalogger and the results stored immediately following the measurements due to limited data storage capacity for raw data. These flux calculations were carried out with the PEC software (Corbari *et al.* 2012) which has been developed for real time average data management. The same corrections as for the camelina site were carried out. A comparison between corrected fluxes from high frequency and from 30 min average data at a different site, notably a maize field in Italy, showed that low errors could be obtained with mean absolute daily difference of 6.1 $\mathrm{W\,m^{-2}}$ for H and 13.2 $\mathrm{W\,m^{-2}}$ for λE (Corbari, unpublished data).

The surface roughness was calculated from the sonic anemometer data for 30°-azimuthal classes by means of the following equation:

$$u = \frac{u_*}{k}\left[\ln\left(\frac{z-d}{z_{0\mathrm{m}}}\right) - \Psi_m\left(\frac{z-d}{L}\right)\right] + \Psi_m\left(\frac{z_{0\mathrm{m}}}{L}\right), \quad (1)$$

where u is the horizontal wind speed [m s^{-1}], u_* the friction velocity [m s^{-1}], $k = 0.41$ the von Kármán constant, z the measurement height [m], d the zero-displacement height [m], and Ψ_m is a stability correction function according to Paulson (1970). For unstable conditions:

$$\Psi_m = 2\ln\left(\left(1+x\right)/2\right) + \ln\left(\left(1+x^2\right)/2\right) - 2\arctan\left(x\right) + \pi/2\ , \quad (2)$$

where (Dyer 1974):

$$x = 1 - 16\left(\frac{z}{L}\right)^{-0.25}\ . \quad (3)$$

For stable conditions:

$$\Psi_m = 1 + 5\frac{z}{L}\ . \quad (4)$$

The friction velocity was calculated as the square root of the covariance of measured vertical and horizontal wind speed, and d was assumed 2/3 of the canopy height for the camelina (a closed crop), and a rough estimate of d of 0.4 m was made based on Fig. 1 in Raupach (1994) for the other two stations (with sparse vegetation). The value of z_{0m} was calculated by minimizing the squared difference between measured (sonic anemometer) and calculated (Eq. 1) horizontal wind speed u. This minimization was carried out on data in 12 classes of wind direction of 30° each, in order to evaluate the roughness in different directions from the towers. This procedure was repeated for different values of d since d was estimated only roughly, but varying d resulted in only very small variations in the calculated z_{0m}.

The source areas of the fluxes were estimated following Hsieh *et al.* (2000) for main wind and Detto *et al.* (2006) for the lateral wind direction. These models require the surface roughness, main wind speed, u, and lateral wind speed, v, vector as input. The flux tower data and the estimated z_{0m} values have been used.

3.2 Soil heat flux

At the camelina site, six ground heat flux plates were installed, while only two were installed on the two other sites. Therefore, the analysis of the soil heat flux was carried out at the camelina site, where below-ground measurements were most elaborate. The soil thermal properties found at this site were thereafter used for the other sites as well, assuming equal thermal soil

properties for all sites, to convert soil heat flux from the measurement depth to the surface (soil types were visibly similar, and soil moisture in the topsoil was very low – around 10% at 10 cm depth, and less near the surface).

For the camelina site, the soil heat flux at the surface was calculated from temperature profile measurements at 6 depths below the surface radiometric surface temperature and the measured heat flux at 8 cm depth. The soil heat flux measured at 13 cm depth was used for validation. All soil temperature sensors were calibrated prior to the campaign.

The 10-day half hourly averaged soil temperature time series at 8 cm depth was fitted to a Fourier series with a number of harmonics of 1/7th of the number of data points. The soil temperatures measured at the other depths together with the radiometric soil temperature were used to tune the diffusivity D [$m^2\,s^{-1}$], used in the thermal diffusion equation of de Vries (1963):

$$\frac{\partial T}{\partial t} = -D\frac{\partial^2 T}{\partial z^2} \tag{5}$$

by minimizing the quadratic difference between measured and modelled soil temperatures. The derivatives of the Fourier series were calculated analytically according to van der Tol (2012). The heat conductivity of the soil, κ [$Wm^{-1}\,K^{-1}$], was solved from

$$G = -\kappa\frac{\partial T}{\partial z} \tag{6}$$

by means of a linear regression of the vertical temperature gradient and the measured heat flux at 8 cm depth. Because it appeared that D and κ were not constant with depth (see results section), separate values for these two soil thermal properties were derived for the depth intervals between consecutive pairs of soil temperature measurements (*e.g.*, 8-4, 4-2 cm depth, *etc.*), working upward and downward away from the 8 cm depth, in order to obtain a better estimate of the soil heat flux with depth, in particular at the surface.

The 10-day average soil temperatures consistently decreased with depth, revealing a downward, seasonal component of the soil heat flux. This seasonal heat flow could not be modelled with the harmonics for this relatively short time series of 10 days. For this reason, the observed 10-day mean values of soil temperature at each depth were subtracted from the observed soil temperatures, such that the soil temperatures corrected for seasonal heat flow had a zero mean at all depths. A similar normalization procedure was carried out to the measured heat fluxes: the 10-day mean soil heat flux was subtracted from the measurements at 8 cm depth prior to fitting the heat conductivity. The fitting procedure described above was applied to these normalized soil temperatures and heat fluxes. The measured 10-day means were added to the modelled temperature time series afterwards.

The heat flux at the surface obtained with the normalized temperatures lacks the seasonal component. The seasonal component was calculated separately from the 10-day average temperatures and heat conductivity using Eq. 3. As a further verification of this procedure, the calculated value of the seasonal heat flux component was compared to the 10-day average value of the measured heat flux at 8 cm depth.

3.3 Energy balance closure

The energy balance was evaluated by regression of $H + \lambda E$ *versus* $R_n - G$. The regression is only meaningful if there is no random error in the independent variable (Wilson *et al.* 2002). Although the random error in $R_n - G$ is probably lower than that in the turbulent heat fluxes, it is not zero. For this reason we also evaluated the EBR: the ratio of the cumulative $H + \lambda E$ over cumulative $R_n - G$.

Because the reforestation lacked a four component radiometer, incoming radiation from the camelina site was used, and airborne data were used to estimate albedo. Flights took place during the campaign, as described in Timmermans *et al.* (2014). The albedo of the reforestation was estimated from spectrally integrated (0.43-2.2 μm), atmospherically corrected reflectance measurements of the airborne hyperspectral scanner (AHS), a hyperspectral mapper in the optical and thermal domain on board of the aircraft. Upwelling longwave radiation was measured with the IRTS Apogee sensor.

3.4 Sensible and latent heat flux from vertical profiles

The temperature and relative humidity sensors used at the camelina site were calibrated against each other across the range of observed temperature and relative humidity values with linear regression. In two cases, second order polynomial fits were required to obtain a satisfactory inter-calibration. The calibration removed the bias and reduced the relative errors induced by differences in sensor sensitivities by 90% to less than 0.06 °C for T and 0.12% for RH for the CS215 sensors used at the camelina site. With this accuracy, S:N ratio of the vertical differences in temperature and humidity increases from approximately 0.5-2.5 to 5-25.

The sensible heat flux was estimated from pairs of temperature and wind speed data as:

$$H_{\mathrm{profile}} = -\rho_a c_p k^2 \frac{\left(T\left(z_i\right) - T\left(z_j\right)\right)\cdot\left(u\left(z_k\right) - u\left(z_l\right)\right)}{\left[\ln\left(\frac{z_i}{z_j}\right) - \Psi_h\left(\frac{z_i}{L}\right) + \Psi_h\left(\frac{z_j}{L}\right)\right]\left[\ln\left(\frac{z_k}{z_l}\right) - \Psi_m\left(\frac{z_k}{L}\right) + \Psi_m\left(\frac{z_l}{L}\right)\right]}\,, \quad (7)$$

where ρ_a is the air density [kg m^{-3}], and c_p the heat capacity of the air [J kg^{-1} K^{-1}], both considered as constants; z_i and z_j are measurement heights of temperature less the zero plane displacement height d; and z_k and z_l measurement heights of wind speed minus d. The Obukhov length L was obtained from the processed eddy covariance data.

Latent heat flux was calculated from H_{profile} with the Bowen ratio, Bo, (Bowen 1926):

$$E_{\text{BR}} = \frac{H_{\text{profile}}}{Bo} , \tag{8}$$

where Bo is calculated from the temperature and humidity measurements at two heights:

$$Bo = \frac{c_p}{\lambda} \frac{T(z_i) - T(z_j)}{q(z_i) - q(z_j)} , \tag{9}$$

where λ is the latent heat for evaporation [J kg^{-1}], and q the specific humidity [kg vapour kg^{-1} air], calculated from air temperature and relative humidity.

3.5 Sensible heat flux from radiometric temperature

Sensible heat flux from radiometric, T_r, and air temperature, H_{rad}, was also calculated with Eq. 4 after replacing $T(z_i)$ by the radiometric temperature T_r, z_i by the roughness height for heat, z_{0h}, and z_k by the roughness height for momentum, z_{0m}. The unknown value of z_{0h} was calibrated by tuning the value of $\ln(z_{0m}/z_{0h})$ to match calculated sensible heat flux with the eddy covariance estimate of sensible heat flux (Stewart *et al.* 1994).

4. RESULTS

4.1 Surface roughness

The roughness length at the flux stations appeared to peak in some specific upwind directions compared to other directions. This was the case at all three flux stations, but the directions in which the peaks occur differed among the sites (Fig. 3). In all cases, the peaks coincided with the position of the gas analyser relative to the sonic anemometer, suggesting that the instrument influenced the roughness estimates by increasing its values. This suggestion is supported by a comparison of the roughness calculated from the measurements of the two sonic anemometers at the camelina site, one without and one with an gas analyser in the vicinity. The roughness length calculated from the anemometer data with gas analyser showed a peak in the direction of the gas analyser (northwest of the anemometer), while the roughness length from the anemometer data without gas analyser did not show this

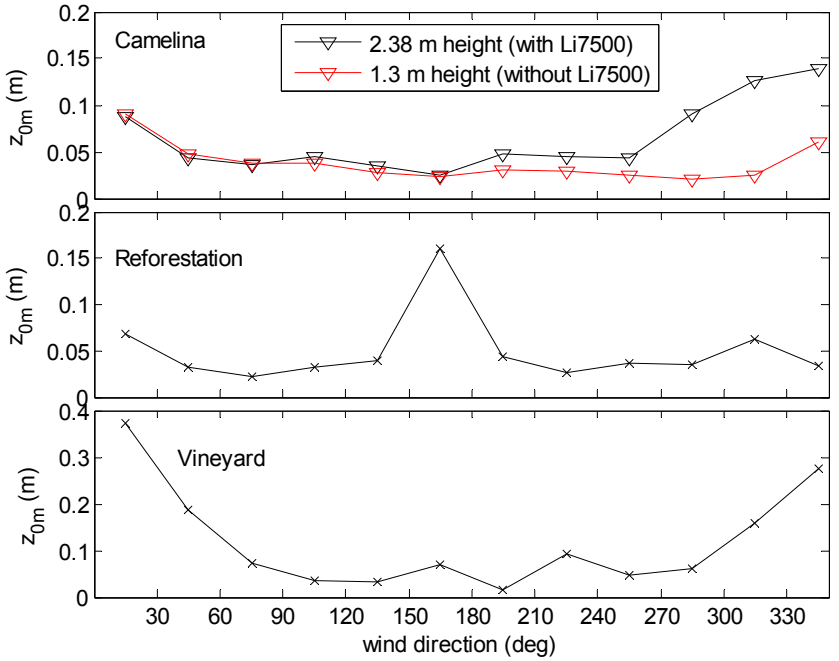

Fig. 3. Variation of roughness length for momentum z_{0m} around the measurement towers with wind direction. LiCor gas analyser positions were: 300° (camelina), 170° (reforestation), and 0° (vineyard).

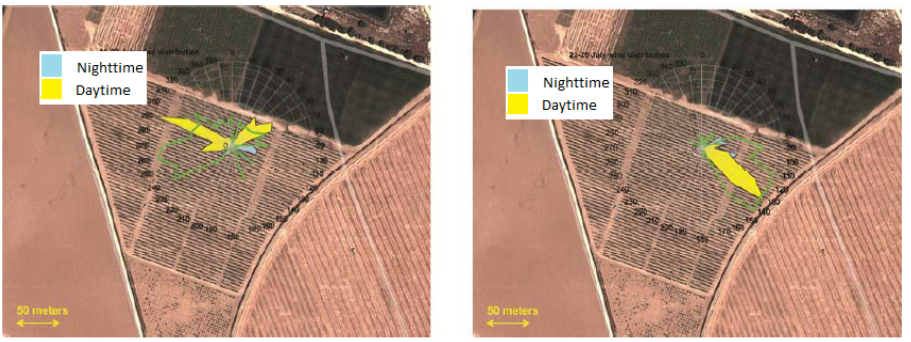

(a) (b)

Fig. 4. Wind conditions at the vineyard site during the campaign. In the period from 19 to 22 July (panel a) daytime wind speed was between 1.5 and 3.0 m/s during 90% of the time, whereas in the second period from 23 to 26 July (panel b) daytime wind speed was higher than 5 m/s during 90% of the time. Prevailing wind directions in the first period were from the north, in the second period from the southeast.

peak. At the camelina site, there is also evidence for a wind shadow caused by the tower: the roughness length appeared higher for wind from the north. Hence, data contaminated by the disturbance of the measured turbulence by the gas analyser and tower were excluded from further analysis.

The situation at the vineyard site is more complicated than at the camelina site, because of the smaller fetch and the orientation of the grape vines in rows (Fig. 4). The airborne color composite in Fig. 4 shows the orientation of the rows from WNW to ESE, and a relatively small fetch in the north direction of 50 m compared to >100 m in other directions. The higher roughness in the north direction (300-60°) suggests that the contrast between the grass field and the vineyard is responsible for the higher roughness in this direction.

4.2 Energy balance closure

Time series of measurements of the three flux stations are shown in Fig. 5. At the reforestation and camelina sites, sensible heat flux was relatively high and latent heat flux low, except for the last 24 hours (DOY 209 to 210), when a rainstorm occurred. At that time, only the camelina station was still operational. Evaporation peaked in the night following the rainstorm, at the expense of negative sensible and soil heat fluxes.

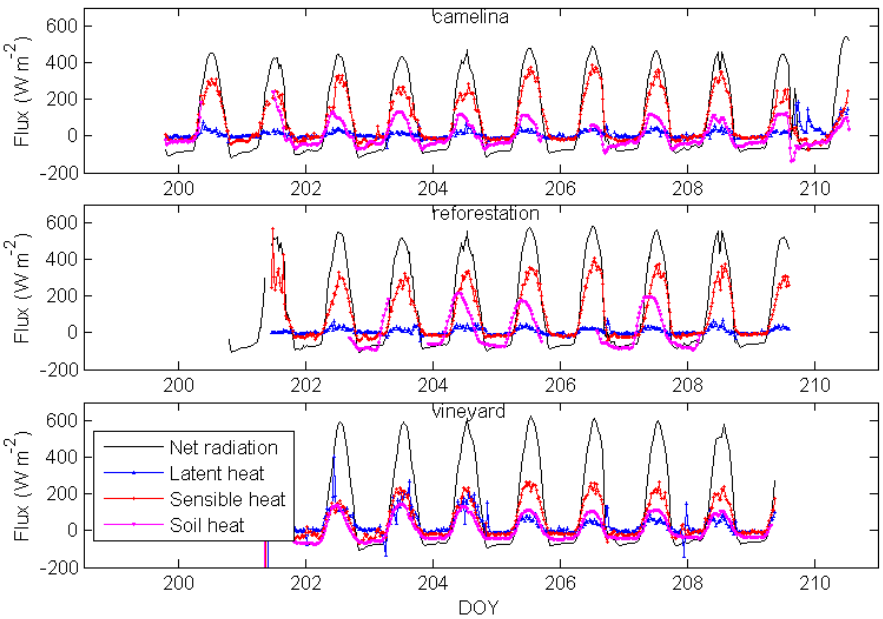

Fig. 5. Thirty-min interval net radiation R_n, ground heat flux G, and turbulent heat fluxes (H and λE) *versus* day of year (DOY) for the three flux stations.

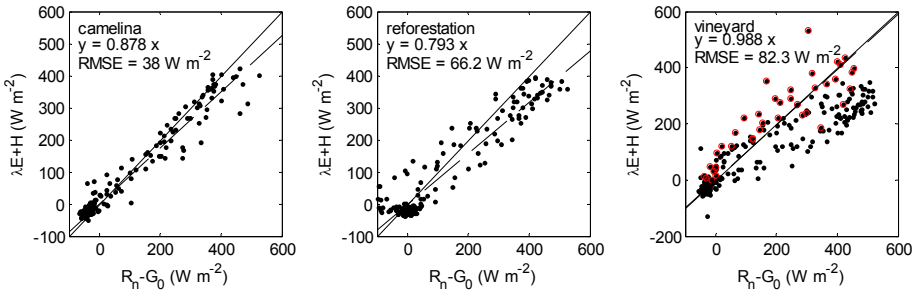

Fig. 6. Thirty-min interval turbulent heat fluxes (H and λE) *versus* available energy ($R_n - G$) for the three flux station sites, with 1:1 lines (solid), and linear regressions forced through the origin (dashed). For the vineyard site, all data are shown (black dots) as well data with an 80% upwind footprint area completely within the vineyard (red circles; ~10% of the data): less than 200 m upwind distance and wind direction from 30 to 330°. RMSE and slope were calculated for the footprint areas completely in the vineyard.

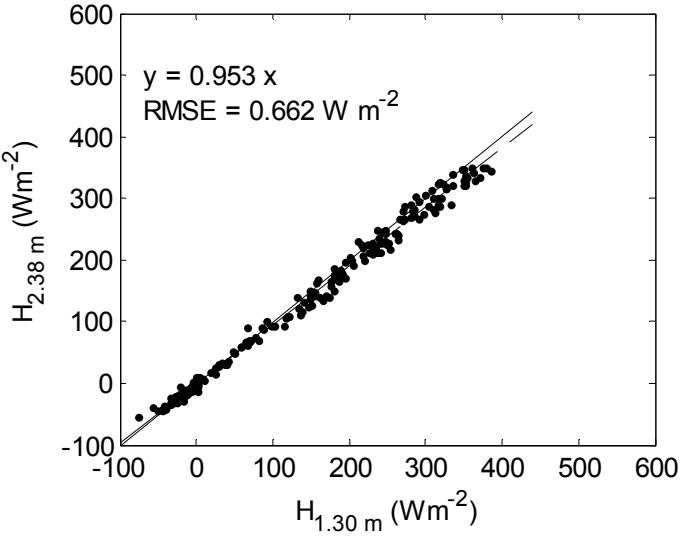

Fig. 7. Comparison of the sensible heat flux measured at the camelina site at two heights, with 1:1 line (solid) and linear regression (dashed).

The overall energy balance closure was 88, 79, and 99% at the camelina, reforestation and vineyard sites, respectively, based on regression of $H - \lambda E$ *versus* $R_n - G_0$, while the EBRs were 1.05, 0.91, and 0.73. The RMSE was 38, 66, and 83 $\mathrm{Wm^{-2}}$ for the half-hourly values of $R_n - H - \lambda E - G_0$ (Fig. 6). The contrasting result for the regression (99% closure) and EBR (73% closure) for the vineyard site is due to the low number of data points (41) in-

cluded. Data with wind directions between 330 and 30° were rejected, as well as data with an 80% upwind footprint area exceeding 200 m. This resulted in 90% of the data being excluded from the calculation. For the camelina and reforestation sites, only the data that were affected by the position of the gas analyser were rejected. At these sites, the 80% footprint area did not extend beyond the field except for a few occasions during stable night-time conditions. At the camelina site, two sonic anemometers were present, at 1.30 and at 2.38 m height, which provided similar results (Fig. 7).

4.3 Soil heat flux

Calibration of the soil heat flux model to the temperature profile and heat flux measurements at the camelina site resulted in a soil heat diffusivity D of $0.273 \times 10^{6}\ \mathrm{m^2\,s^{-1}}$, heat conductivity κ of $0.359\ \mathrm{W m^{-1}\,K^{-1}}$, and volumetric heat capacity c_p of $1.32 \times 10^{6}\ \mathrm{J\,m^{-3}\,K^{-1}}$; the latter value corresponds to a volumetric soil moisture content of 6 at 40% porosity, following de Vries (1963).

An evaluation of the modelled temperature profile indicated that these thermal properties could not have been constant with depth. With a single value for D and another for κ fitted for the entire soil profile (0-32) cm, the temperature curves for the top 4 cm could not be reproduced: the model overestimates the phase shift and underestimates the amplitude shift. Fitting the thermal properties separately for each pair of sensors at consecutive depth improved the correspondence of measured and modeled temperature (Fig. 8), and, more importantly, led to a more realistic phase of the ground heat flux diurnal cycle while the amplitude was hardly affected by vertically changing thermal properties. The resulting thermal conductivity in the upper 1 cm was an order of magnitude higher and the heat capacity an order of magnitude lower than that deeper in the soil. The RMSE of the closure term was reduced by $16\ \mathrm{W\,m^{-2}}$ when the soil thermal properties were varied with depth.

It should be noted that the radiometric surface temperatures had a diurnal amplitude equal to that at 1 cm depth, and midday values that were sometimes lower than those at 1 cm depth. One would expect the opposite: a higher amplitude and consistently higher daytime temperatures at the surface. An error in the emissivity value of 0.945, tuned to match the 10-day mean radiometric temperature and the 10-day mean of the temperature at 1 cm depth, could not explain the difference in amplitude. The most obvious explanation for the relatively low amplitude is the fact that radiometric temperature includes contributions from the vegetation, which was exposed to turbulence in the vegetation layer and which is affected by cooling due to transpiration (although the latent heat flux was low the crop was senescent).

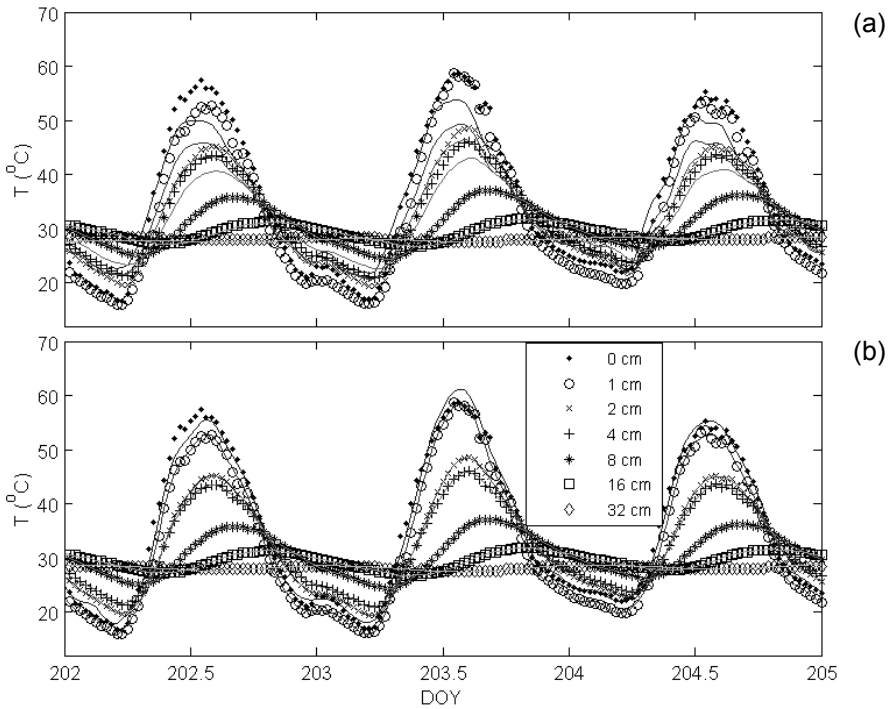

Fig. 8. Measured (symbols) and modelled (lines) time series of soil temperature at the camelina site for part of the measurement campaign, with constant thermal properties with depth (a), and with thermal properties that varied with depth (b).

4.4 Turbulent heat fluxes from temperature, humidity, and wind profiles

Although vertical differences in air temperature were low at the camelina site (Fig. 9), they were large enough to estimate sensible heat flux (Eq. 7) and latent heat flux (Eq. 8). For temperature and humidity, the heights of 2.20 and 1.20 m were used, closest to the wind speed, and friction velocity measurements at 1.35 and 2.58 m height. Modelled H and λE match well with observations (RMSE of 60 and 38 W m^{-2}, respectively), even during the last 24 hours of the measurement period in which rainfall occurred (Figs. 10 and 11).

Of particular importance are the terms Ψ_h and Ψ_m in Eq. 7 for stability. Omitting these terms (*i.e.*, assuming neutral conditions) would result in a RMSE of 90 W m^{-2} for the sensible heat flux, and a slope of the linear regression between measured and modelled H of 1.8 (*i.e.*, underestimate of sensible heat flux) due to very unstable conditions at the camelina site. Here the functions Ψ_h and Ψ_m had been obtained from the eddy covariance data of

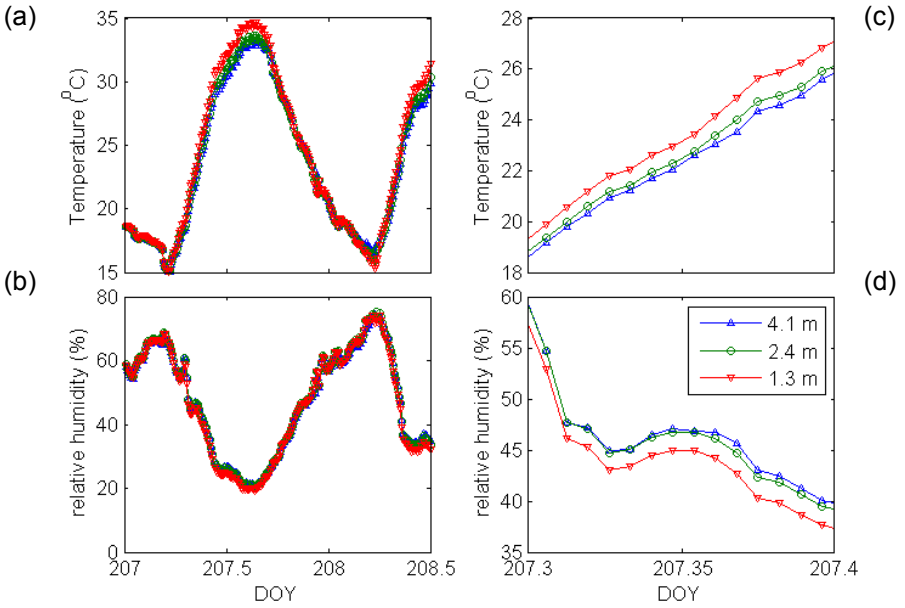

Fig. 9. Air temperature (a, c) and relative humidity (b, d) profiles at the camelina site during the day of overpass (a, b), and zoomed in for the hours of the overpass.

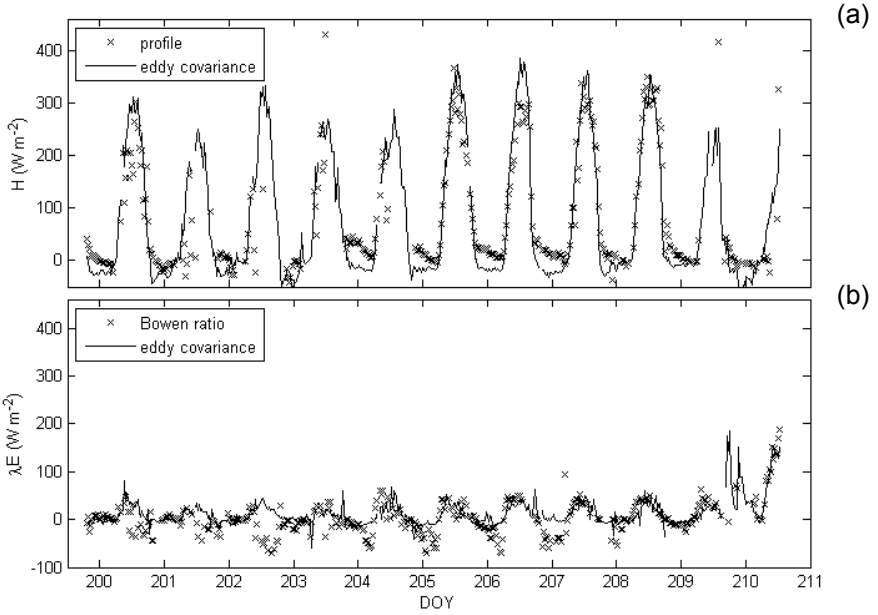

Fig. 10. Profile (Eq. 7) modelled sensible heat flux (a) and Bowen ratio derived latent heat flux (b) at the camelina site *versus* day of the year 2012, both with their equivalents derived from eddy covariance and gas exchange measurements directly.

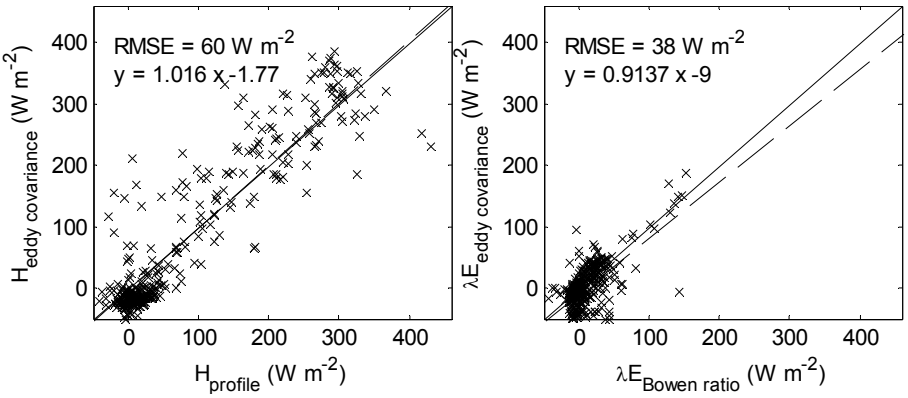

Fig. 11. The data of Fig. 10 presented as scatter plots, with 1:1 line (solid) and linear regression (dashed).

friction velocity and stability. These two variables can also be obtained iteratively from modelled H and the temperature and wind profiles. Doing so results in a RMSE of H of 64 W m^{-2}, somewhat higher than using the eddy covariance data, but much better than when omitting the stability corrections.

During most of the nights, the profile data show negative H, which is in agreement with the eddy covariance estimates. In four warmest nights (DOY 204 to 207), the temperature profile was reversed: the highest temperatures at the lowest level (1.3 m) and the lowest temperature at the highest level (4.3 m), which would mean that unstable conditions and positive H continued during the night. The eddy covariance estimates of H were nevertheless negative during these nights. It should be noted that during these relatively warm nights, the temperature differences between the sensors were as low as 0.1 °C, while the measurement error was up to 0.06 °C.

Applying the same procedure to the reforestation and vineyard sites (not shown) resulted in RMSE of sensible heat flux of 277 and 242 W m^{-2}, respectively. These much higher errors are related to both the lower signal to noise ratio of the data (the sensors were not inter-calibrated), and the fact that the temperature profiles may be affected by advection.

4.5 Sensible heat flux from radiometric surface temperature

The sensible heat flux calculated from radiometric temperature varied widely with the value of the parameter $kB^{-1} = \ln(z_{0m}/z_{0h})$, where B is the Stanton number at the camelina site. At the value $kB^{-1} = 17$, the RMSE of modelled H had a minimum, and eddy covariance sensible heat flux was well reproduced (Fig. 12), but at values of kB^{-1} below 10, the RMSE quickly rose to

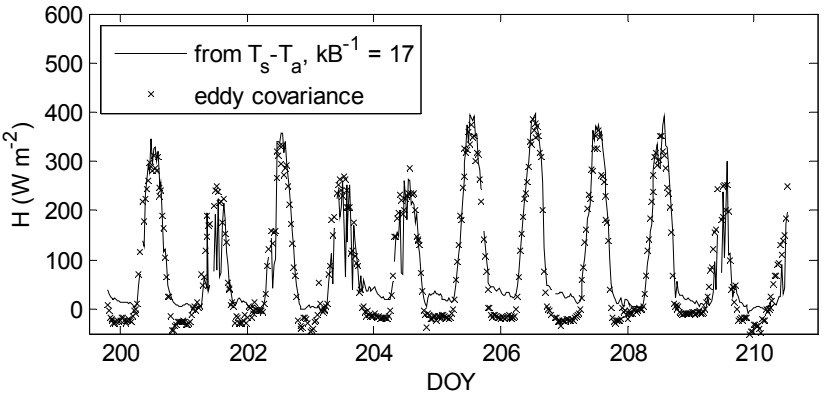

Fig. 12. Time series of sensible heat flux calculated from the difference between radiometric surface temperature and air temperature (symbols) and eddy covariance derived sensible heat flux at the camelina site.

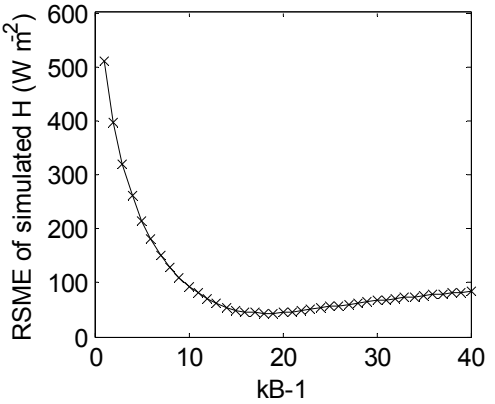

Fig. 13. Effect of the parameter kB^{-1} on the RMSE of simulated heat fluxes at the camelina site, for the whole time series of the experiment.

unrealistic values (Fig. 13). The parameter kB^{-1}, first introduced by Owen and Thomsom (1963), is known to vary, especially in areas with partial vegetation cover: Stewart *et al.* (1994) found values between 3.5 and 12.5 for grass, forest, rocks, and savannah sites, all in arid regions. Verhoef *et al.* (1997) found a similar range for savannahs in Africa. They argued that kB^{-1} is not only difficult to estimate, but that even the approach of extrapolating the temperature profile to the radiometric surface temperature is questionable. Physically based models are able to capture the full range of kB^{-1} values (Massman 1999, Su *et al.* 2001). These models require knowledge of the drag and heat transfer coefficients of leaves. Reproducing the high value of

kB^{-1} of 17 with the model of Massman (1999) requires an exceptionally low heat transfer coefficient of the leaf. The parameter kB^{-1} may also vary with time (Yang *et al.* 2003), but in the present study with fairly constant weather conditions and soil moisture, the sensible heat fluxes could be reproduced well with a single value for kB^{-1}.

4.6 Effects of a rainfall event

A rainfall event (including hail) of 14.1 mm on the last day of the measurement campaign (evening of DOY 209) caused some interesting features in the time series. For example, the radiometric surface temperature at the camelina site dropped by 30 °C within half an hour to a value below air temperature. The rain event was followed by high night-time evaporation rates that varied concomitant with wind speed. The energy for evaporation was partly supplied by negative sensible and soil heat fluxes (soil thermal properties obviously changed during the rainfall event, but they could not be calibrated for periods shorter than a day), leaving a relatively small energy balance closure gap (~30 W m^{-2}, see Fig. 14).

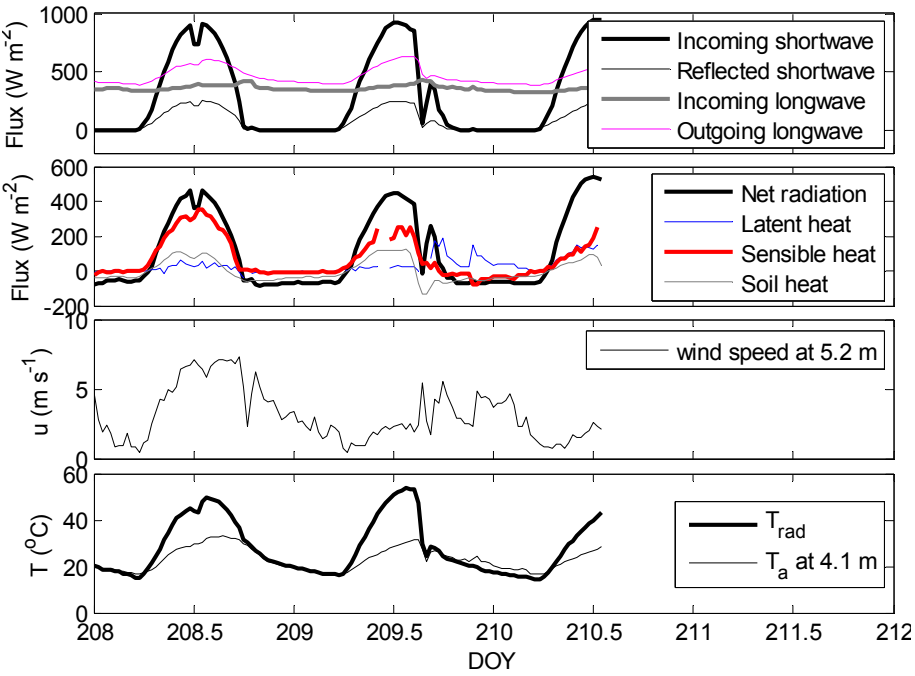

Fig. 14. Time series of radiation components, heat fluxes, wind speed and radiometric surface, and air temperature (at the camelina site on the day before the rainfall event, the day of the rainfall event, and the day following the rainfall event).

5. DISCUSSION

The energy balance closure gap was smallest in the most homogeneous site (camelina), and largest in the most heterogeneous site with limited fetch (vineyard). The closure gap in the camelina site is small compared to most published values (*e.g.*, Wilson *et al.* 2002, Foken 2008), and too small to identify its source. Obvious factors that are known to adversely affect the energy balance (Foken 2008, Liebethal *et al.* 2005) have been ruled out at this site: (i) the calculation of ground heat flux at the surface, (ii) application of frequency response correction of the turbulent fluxes, and (iii) calibration of the radiometer. We considered including heat storage in the vegetation and air layer up to the level of the sensors in the energy balance equation, but calculated heat storage changes appeared to be negligible due to the low biomass and low measurement height. The remaining errors in closure could be due to measurement or representation errors of the turbulent heat fluxes. The EBR suggested a small overestimate of the turbulent fluxes, whereas the linear regression of half hourly estimates suggested a small underestimate. Frank *et al.* (2013) recently showed that the sonic anemometer that was used (CSAT3), due to its design, may underestimate vertical wind speed and thus sensible heat flux by 8%. Although their study was carried out over forest, we could not exclude the possibility that our sensible heat fluxes are underestimated as well.

The small energy balance closure gap at the camelina site gives confidence in the flux tower data. Moreover, the calculated 80% source area of the fluxes did not extend beyond the edges of the camelina field for either of the two measurement heights (not shown) except for a small number of night-time cases, only two of which included an irrigated field. Moreover, the sensible heat flux measurements at both heights were almost equal (Fig. 7). This confirms that the measurements represent the local fluxes for the camelina site. Nevertheless, we cannot rule out that larger scale thermally induced circulations contributed to the locally measured flux. At larger spatial scale, both in horizontal and vertical direction, we expect large eddies to contribute to the advection and circulation of heat due to strong contrasts in vegetation cover, soil moisture, and surface temperatures. The measurements at the camelina site were carried out in a field with nearby irrigated plots, which could cause such mesoscale eddies and a non-zero stationary vertical wind speed (*e.g.*, Foken 2008, Eder *et al.* 2015). The average uncorrected vertical wind speed over the entire period was 4 $cm^2 s^{-1}$ in upward direction, which indicates that the site had either convective rising, or that the anemometer was slightly misaligned.

At the vineyard site, a more detailed footprint calculation is required to obtain local surface fluxes. A first analysis showed that in 90% of the half-

hourly intervals, the 80% upwind footprint area included other fields. In the first 5 days of the measurement campaign, the wind was predominantly from the north and the flux footprint extended to an adjacent irrigated grass field. In calculating energy balance statistics, these data were excluded. Another problem of the footprint calculation is that the models that were used are not valid for footprints that have a variable roughness in space.

At the camelina site, sensible and latent heat flux could accurately be reproduced with the wind profile in combination with Bowen ratios. This was not the case at the reforestation and vineyard sites, where gradients were not always consistent with eddy covariance fluxes (even if considering larger uncertainty in the data due to the fact that the sensors in the vertical profiles at these sites were not inter-calibrated). This indicates that the fluxes at these two sites were not only local fluxes.

The sensible heat flux at the camelina site could be accurately reproduced from the difference between radiometric surface temperature and air temperature, but only when using a considerable excess resistance for heat, kB^{-1}, higher than most reported values (Gökmen *et al.* 2012). The lack of a physical basis for the roughness height for heat z_{0h} makes it a tuning parameter.

Acknowledgments. The research leading to these results has received funding from the European Community's 7th Framework Programme (FP7/2008-2013) under EUFAR contract no. 227159, Cost Action ES0903-EUROSPEC and ESA Grant D/EOP/rp/2012/48. Murat Uçer and Xuelong Chen (University of Twente) provided assistance in the field. Two anonymous reviewers provided suggestions that have been used to improve the paper.

References

Bowen, I.S. (1926), The ratio of heat losses by conduction and by evaporation from any water surface, *Phys. Rev.* **27**, 6, 779-787, DOI: 10.1103/PhysRev.27.779.

Cleugh, H.A., R. Leuning, Q. Mu, and S.W. Running (2007), Regional evaporation estimates from flux tower and MODIS satellite data, *Remote Sens. Environ.* **106**, 3, 285-304, DOI: 10.1016/j.rse.2006.07.007.

Corbari, C., D. Masseroni, and M. Mancini (2012), Effetto delle correzioni dei dati misurati da stazioni eddy covariance sulla stima dei flussi evapotraspirativi, *Ital. J. Agrometeorol.* **1**, 35-51 (in Italian).

de Vries, D.A. (1963), Thermal properties of soils. **In:** W.R. van Wijk (ed.), *Physics of Plant Environment*, North-Holland Publ. Co., Amsterdam.

Detto, M., N. Montaldo, J.D. Albertson, M. Mancini, and G. Katul (2006), Soil moisture and vegetation controls on evapotranspiration in a heterogeneous Mediterranean ecosystem on Sardinia, Italy, *Water Resour. Res*. **42**, 8, W08419, DOI: 10.1029/2005WR004693.

Dyer, A.J. (1974), A review of flux-profile relationships, *Bound.-Lay. Meteorol*. **7**, 3, 363-372, DOI: 10.1007/BF00240838.

Eder, F., M. Schmidt, T. Damian, K. Träumner, and M. Mauder (2015), Mesoscale eddies affect near-surface turbulent exchange: evidence from lidar and tower measurements, *J. Appl. Meteorol. Clim.* **54**, 1, 189-206, DOI: 10.1175/JAMC-D-14-0140.1.

Foken, T. (2008), The energy balance closure problem: An overview, *Ecol. Appl.* **18**, 6, 1351-1367, DOI: 10.1890/06-0922.1.

Foken, T., M. Göckede, M. Mauder, L. Mahrt, B. Amiro, and W. Munger (2005), Post-field data quality control. **In:** X. Lee, W. Massman, and B. Law (eds.), *Handbook of Micrometeorology*, Atmospheric and Oceanographic Sciences Library, Vol. 29, Springer Netherlands, 181-208, DOI: 10.1007/1-4020-2265-4_9.

Frank, J.M., W.J. Massman, and B.E. Ewers (2013), Underestimates of sensible heat flux due to vertical velocity measurement errors in non-orthogonal sonic anemometers, *Agr. Forest Meteorol*. **171-172**, 72-81, DOI: 10.1016/j.agrformet.2012.11.005.

Gash, J.H.C. (1987), An analytical framework for extrapolating evaporation measurements by remote sensing surface temperature, *Int. J. Remote Sens.* **8**, 8, 1245-1249, DOI: 10.1080/01431168708954769.

Gökmen, M., Z. Vekerdy, A. Verhoef, W. Verhoef, O. Batelaan, and C. van der Tol (2012), Integration of soil moisture in SEBS for improving evapotranspiration estimation under water stress conditions, *Remote Sens. Environ*. **121**, 261-274, DOI: 10.1016/j.rse.2012.02.003.

Hsieh, C.I., G. Katul, and T.W. Chi (2000), An approximate analytical model for footprint estimation of scalar fluxes in thermally stratified atmospheric flows, *Adv. Water Res.* **23**, 7, 765-772, DOI: 10.1016/S0309-1708(99)00042-1.

Horst, T.W. (1997), A simple formula for attenuation of eddy fluxes measured with first-order-response scalar sensors, *Bound.-Lay. Meteorol*. **82**, 2, 219-233, DOI: 10.1023/A:1000229130034.

Kalma, J.D., T.R. McVicar, and M.F. McCabe (2008), Estimating land surface evaporation: A review of methods using remotely sensed surface temperature data, *Surv. Geophys.* **29**, 4-5, 421-469, DOI: 10.1007/s10712-008-9037-z.

Kustas, W.P., and J.M. Norman (1996), Use of remote sensing for evapotranspiration monitoring over land surfaces, *Hydrol. Sci. J.* **41**, 4, 495-516, DOI: 10.1080/02626669609491522.

Kustas, W.P., K.S. Humes, J.M. Norman, and M.S. Moran (1996), Single- and dual-source modeling of surface energy fluxes with radiometric surface temperature, *J. Appl. Meteorol. Clim.* **35**, 1, 110-121, DOI: 10.1175/1520-0450(1996)035<0110:SADSMO>2.0.CO;2.

Liebethal, C., B. Huwe, and T. Foken (2005), Sensitivity analysis for two ground heat flux calculation approaches, *Agr. Forest Meteorol*. **132**, 3-4, 253-262, DOI: 10.1016/j.agrformet.2005.08.001.

Massman, W.J. (1999), A model study of kB_H^{-1} for vegetated surfaces using 'localized near-field' Lagrangian theory, *J. Hydrol.* **223**, 1-2, 27-43, DOI: 10.1016/S0022-1694(99)00104-3.

Owen, P.R., and W.R. Thomson (1963), Heat transfer across rough surfaces, *J. Fluid Mech.* **15**, 3, 321-334, DOI: 10.1017/S0022112063000288.

Paulson, C.A. (1970), The mathematical representation of wind speed and temperature profiles in the unstable atmospheric surface layer, *J. Appl. Meteorol. Clim*. **9**, 6, 857-861, DOI: 10.1175/1520-0450(1970)009<0857:TMROWS>2.0.CO;2.

Raupach, M.R. (1994), Simplified expressions for vegetation roughness length and zero-plane displacement as functions of canopy height and area index, *Bound.-Lay. Meteorol.* **71**, 1-2, 211-216, DOI: 10.1007/BF00709229.

Schotanus, P., F.T.M. Nieuwstadt, and H.A.R. de Bruin (1983), Temperature measurement with a sonic anemometer and its application to heat and moisture fluxes, *Bound.-Lay. Meteorol.* **26**, 1, 81-93, DOI: 10.1007/BF00164332.

Stewart, J.B., W.P. Kustas, K.S. Humes, W.D. Nichols, M.S. Moran, and H.A.R. de Bruin (1994), Sensible heat flux-radiometric surface temperature relationship for eight semiarid areas, *J. Appl. Meteorol. Clim.* **33**, 9, 1110-1117, DOI: 10.1175/1520-0450(1994)033<1110:SHFRST>2.0.CO;2.

Su, Z., T. Schmugge, W.P. Kustas, and W.J. Massman (2001), An evaluation of two models for estimation of the roughness height for heat transfer between the land surface and the atmosphere, *J. Appl. Meteorol. Clim.* **40**, 11, 1933-1951, DOI: 10.1175/1520-0450(2001)040<1933:AEOTMF>2.0.CO;2.

Su, Z., W. Timmermans, A. Gieske, L. Jia, J.A. Elbers, A. Olioso, J. Timmermans, R. van der Velde, X. Jin, H. van der Kwast, F. Nerry, D. Sabol, J.A. Sobrino, J. Moreno, and R. Bianchi (2008), Quantification of land–atmosphere exchanges of water, energy and carbon dioxide in space and time over the heterogeneous Barrax site, *Int. J. Remote Sens*. **29**, 17-18, 5215-5235, DOI: 10.1080/01431160802326099.

Timmermans, W.J., G. Bertoldi, J.D. Albertson, A. Olioso, Z. Su, and A.S.M. Gieske (2008), Accounting for atmospheric boundary layer variability on flux estimation from RS observations, *Int. J. Remote Sens.* **29**, 17-18, 5275-5290, DOI: 10.1080/01431160802036383.

Timmermans, W.J., C. van der Tol, J. Timmermans, M. Ucer, X. Chen, L. Alonso, J. Moreno, A. Carrara, R. Lopez, F. de la Cruz Tercero, H.L. Corcoles, E. de Miguel, J.A.G. Sanchez, I. Pérez, B. Franch, J.-C.J. Munoz, D. Skokovic, J. Sobrino, G. Soria, A. MacArthur, L. Vescovo, I. Reusen, A. Andreu, A. Burkart, C. Cilia, S. Contreras, C. Corbari, J.F. Calleja, R. Guzinski, C. Hellmann, I. Herrmann, G. Kerr, A.-L. Lazar, B. Leutner, G. Mendiguren, S. Nasilowska, H. Nieto, J. Pachego-Labrador, S. Pulanekar, R. Raj, A. Schikling, B. Siegmann, S. von Bueren, and Z.B. Su (2015), An overview of the Regional Experiments for Land-atmosphere Exchanges 2012 (REFLEX 2012) campaign, *Acta Geophys.* **63**, 6, 1465-1484, DOI: 10.2478/s11600-014-0254-1 (this issue).

van der Tol, C. (2012), Validation of remote sensing of bare soil ground heat flux, *Remote Sens. Environ*. **121**, 275-286, DOI: 10.1016/j.rse.2012.02.009.

Verhoef, A., H.A.R. de Bruin, and B.J.J.M. van den Hurk (1997), Some practical notes on the parameter kB^{-1} for sparse vegetation, *J. Appl. Meteorol. Clim.* **36**, 5, 560-572, DOI: 10.1175/1520-0450(1997)036<0560:SPNOTP>2.0.CO;2.

Webb, E.K., G.I. Pearman, and R. Leuning (1980), Correction of flux measurements for density effects due to heat and water vapour transfer, *Quart. J. Roy. Meteorol. Soc*. **106**, 447, 85-100, DOI: 10.1002/qj.49710644707.

Wilson, K., A. Goldstein, E. Falge, M. Aubinet, D. Baldocchi, P. Berbigier, C. Bernhofer, R. Ceulemans, H. Dolman, C. Field, A. Grelle, A. Ibrom, B.E. Law, A. Kowalski, T. Meyers, J. Moncrieff, R. Monson, W. Oechel, J. Tenhunen, R. Valentini, and S. Verma (2002), Energy balance closure at FLUXNET sites, *Agr. Forest Meteorol*. **113**, 1-4, 223-243, DOI: 10.1016/S0168-1923(02)00109-0.

Yang, K., T. Koike, and D. Yang (2003), Surface flux parameterization in the Tibetan Plateau, *Bound.-Lay. Meteorol.* **106**, 2, 245-262, DOI: 10.1023/A:1021152407334.

Received 12 May 2014
Received in revised form 8 August 2015
Accepted 22 October 2015